17th World Conference on Earthquake Engineering, 17WCEE
Sendai, Japan - September 13th to 18th 2020

A TWO-STAGE SEISMIC DESIGN FOR OUTRIGGER STIFFNESS BASED ON INTERSTORY DRIFT RATIO AND OVERTURNING MOMENT RATIO

X. Lai, Z. He[(1)], G. Huang[(2)]

(1) *Corresponding author, Professor, State Key Laboratory of Coastal and Offshore Engineering, Dalian University of Technology, Dalian, China hezheng@dlut.edu.cn*

(2) *Senior Engineer, China Machinery International Engineering Design & Research Institute Co., Ltd,Changsha, China huangguohui@cmie.cn*

Abstract

A two-stage seismic design strategy for the stiffness of outriggers is proposed in this paper to consider the lateral stiffness and the resistance to the progressive collapse of super high-rise buildings. The maximum elastic inter-story drift ratio (EIDR) and the resisted overturning moment ratio of frame to the whole structure at the bottom ($OMRF_0$) are selected as indices of structural performance. The uniform coupled flexural-shear model (FSM) and the swing model (SM) are used to estimate the maximum EIDR and $OMRF_0$, respectively. With the statistical relations for the first two periods from 124 super high-rise frame core-tube buildings, the target maximum EIDR is achieved by designing the first two vibration periods. To reveal the relation between the uniform FSM and the frame-core tube structure (FCTS), the sensitivity analysis of parameters of the uniform FSM to the parameters of the frame-core tube structure (FCTS) is carried out based on a specific super high-rise structure, and corresponding approximate relations are obtained by regression. The results show that the flexural stiffness of the interior core tube (ICT) and the axial stiffness of the exterior frame column (EFC) are the most important factors on the shape of the structural lateral deformation and overall structural lateral stiffness. And the flexural stiffness in the uniform FSM is mainly contributed by the flexural stiffness of ICT. With the help of the regressed relations, the stiffness of the outrigger is designed in the second stage with almost constant EIDR. The feasibility of the proposed strategy is demonstrated by the application to a 258m super high-rise building. The proposed strategy defines the main design objectives for each stage, which also makes the design of stiffness of outriggers more reasonable and efficient.

Keywords: outrigger; seismic design; inter-story drift ratio; frame-core tube structure; overturning moment.

1. Introduction

For seismic design of super high-rise buildings with the frame-core tube structure (FCTS), the maximum elastic inter-story drift ratio (EIDR) and the ratio between the resisted overturning moment of frame to that of the whole structure at the bottom ($OMRF_0$) are typical indices of the lateral stiffness and the resistance to progressive collapse. Outriggers can effectively increase the lateral stiffness by connecting the interior core tube (ICT) to the exterior frame column (EFC). Considering the design requirements related to architectural functions such as the refuge story and the equipment story, the locations of outriggers are greatly restricted, which leads to little space for optimization. In contrast, the reasonable estimate of the stiffness of outriggers is more important for the structural design of super high-rise structures, which normally requires a long design period.

The swing model (SM) (see Fig. 1) can be used to estimate the displacement of super high-rise buildings with outriggers under multiple load patterns[1]. However, there is few analytical solutions to the vibration periods and mode shapes of the SM, which is pretty essential to obtain an accurate estimate of EIDR. Compared with the SW, the coupled flexural-shear model[2] (FSM), in which a shear beam and a flexural beam are connected in parallel via axially rigid links (see Fig. 2), is able to provide an efficient estimate on the elastic response demand of structures excited by earthquakes. For the uniform FSM[3], the mode shapes and ratios of periods with different orders are dominated by a single parameter. Based on this, Miranda and Akkar[4] developed the generalized inter-story drift spectrum to include various lateral deformation pattern, which is further used for estimate of maximum EIDR under near-fault pulse-like ground motions[5]. Although FSMs with non-uniform stiffness were proposed successively[3],[6], deterministic methods to calibrate parameters in these FSMs are not provided in relevant literature.

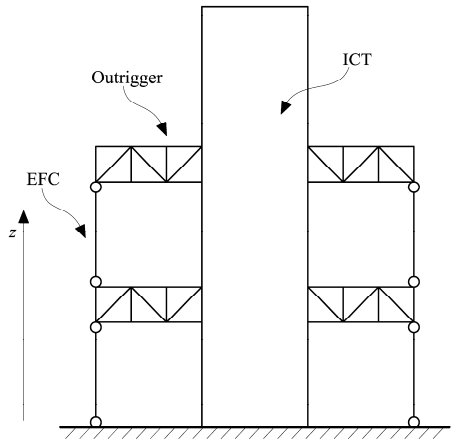

Fig. 1 – Swing model (SM)

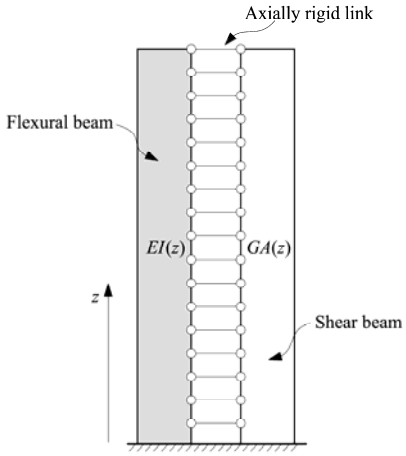

Fig. 2 – Continuum flexural-shear model (FSM)

Not like SW, FSM cannot estimate the internal forces of each sub-system within a structure. In this paper, a two-stage preliminary seismic design strategy of stiffness of outrigger based on the target maximum EIDR and $OMRF_0$ is proposed. Based on specific assumptions, the uniform FSM is used to estimate the EIDR combined with the design response spectrum, and the target maximum EIDR is achieved in the first stage. In terms of the uniform FSM, the key stiffness of the main structural components in the FCTS is determined, and the corresponding approximate relations are built. On the premise of keeping the parameters of the uniform FSM unchanged, the target $OMRF_0$ is achieved by designing the stiffness of outriggers. Finally, the proposed design strategy is applied to a super high-rise building to demonstrate its feasibility.

2. Case-based relation between FSM and FCTS

2.1 Basic information

The super high-rise building with the FCTS in Fig. 3 is used to explore the relation between the uniform FSM and the parameters of main structural components. In addition to the 3D structural model, Fig. 3 also includes the plane layout of the typical strengthened story, the type of outriggers, and the sections and materials of the diagonal brace (DB), the external frame column (EFC) and the core tube (ICT). The concrete-filled steel tubular column is adopted to the EFC, while the steel reinforced concrete wall is adopted to the ICT. The finite element model is built in ETABS[7], in which beams, columns and DBs are simulated by the frame element, while shear walls and slabs are simulated by the shell element. The spectral acceleration is determined according to the Chinese design response spectrum[8] and its extension[9] (see Fig. 4). The characteristic period of the site, i.e. T_g, is 0.55s. The damping ratio ζ is equal to 0.03. The maximum spectrum acceleration $S_{a,max}$ is 2.83m/s^2.

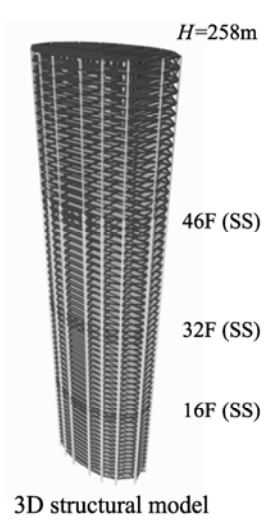

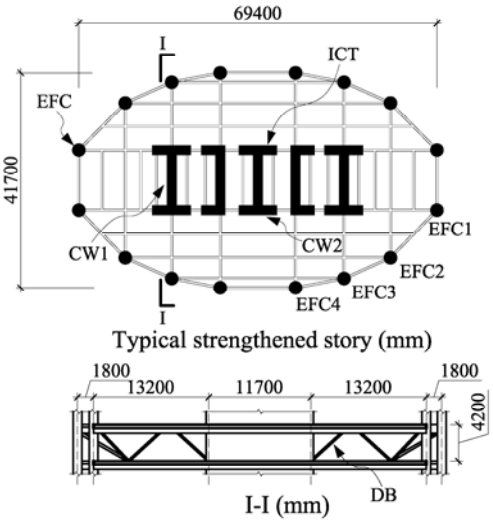

Basic information of structural members:

1) ICT:

Parameters	thickness (mm)		length (mm)		Material	Number	
	1st	61st	1st	61st		1st	61st
CW1	800	500	11700	3000	C60	5	5
CW2	700	400				16	12

Note: the steel ratios in CW1 are 2.41% and 3.85% at the 1st and 61st floor; the steel ratios in CW2 are 5.37% and 9.40% at the 1st and 61st floor.

2) EFC:

Parameters	Outer radius (mm)		Inner radius (mm)		d (mm)	Material	
	1st	61st	1st	61st	C60	1st	61st
EFC1	800	500	755	450	5850	Q345, C60	C60
EFC2	750	500	720	470	15050		
EFC3	750	500	715	470	19050		
EFC4	800	500	755	450	20850		

3) DB:

Q345, A_{DB}=30400mm^2

Fig. 3 – Model information

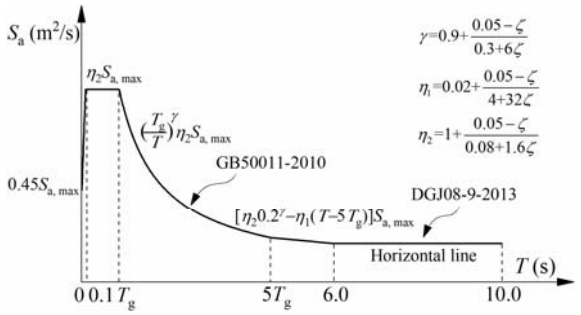

Fig. 4 – Design acceleration response spectrum

2.2 Parameter calibration of uniform FSM

Some basic assumptions for super high-rise buildings should be made before using the uniform FSM, i.e. 1) horizontally regular, symmetrical structural plane layout and the torsional effect can be neglected. A simplified 2D model can be applied; 2) vertical irregularities are not significant and the distributions of lateral stiffness and story mass along structural height can be approximately described by continuous functions; 3) compared with the variation of local lateral stiffness, the outriggers in the strengthened stories (SSs) are mainly used to control the overall lateral stiffness of the structure; 4) for super high-rise buildings whose plane sizes keep constant along the height, the non-uniformity of mass and lateral stiffness distribution along the height is not severe. Corresponding influence on the period ratios and mode shapes is slight.

As the flexural stiffness and shear stiffness in the FSM are contributed by multiple types of structural components, it is difficult to build a one-to-one relation between the previous two stiffness and parameters of structural components. The mode shapes and period ratios of the uniform FSM are only correlated with α_0, which is the non-dimensional ratio of shear stiffness to flexural stiffness as follows[10]:

$$\alpha_0 = H\sqrt{\frac{GA_0}{EI_0}} \tag{1}$$

Where, GA_0 and EI_0 are flexural stiffness and shear stiffness of the uniform FSM, respectively.

Due to the dominant contribution of the first two modes to structural responses, the first two vibration periods can be adopted to calibrate the parameters of the uniform FSM[11]. The period ratio of the j^{th} and i^{th} vibration periods can be obtained[3] as follows:

$$\frac{T_j}{T_i} = \frac{\chi_i}{\chi_j}\sqrt{\frac{\chi_i^2+\alpha_0^2}{\chi_j^2+\alpha_0^2}} \tag{2}$$

Where, T_i is the i^{th} vibration periods.

χ_i is the i^{th} characteristic parameter only related to α_0, which is the solution to the following nonlinear equation[3]:

$$2+\left[2+\frac{\alpha_0^4}{\chi_i^2\left(\alpha_0^2+\chi_i^2\right)}\right]\cos\left(\chi_i\right)\cosh\left(\sqrt{\alpha_0^2+\chi_i^2}\right)+\left[\frac{\alpha_0^2}{\chi_i\sqrt{\alpha_0^2+\chi_i^2}}\right]\sin\left(\chi_i\right)\sinh\left(\sqrt{\alpha_0^2+\chi_i^2}\right)=0 \tag{3}$$

Frankly speaking, such calibration cannot guarantee the prediction accuracy of the periods above the 2nd order and corresponding mode shapes, but still could reflect the influence of structural scheme change on the shape of lateral deformation. The linear density of the uniform FSM can be approximated by the ratio of the total mass to the structural height. When α_0 is determined, EI_0 can be obtained with the same T_1 as the super high-rise building. The i^{th} circular frequency of free vibration of the uniform FSM is shown as follows[3]:

$$\omega_i^2 = \frac{EI_0}{\rho_0 H^4}\chi_i^2\left(\chi_i^2+\alpha_0^2\right) \tag{4}$$

Where, ρ_0 is the linear density of the uniform FSM.

Table 1 shows the first five vibration periods of the finite element model (FEM) and the corresponding uniform FSM. It can be seen that the sums of modal participation mass coefficients of the first five modes of the FEM and the uniform FSM are both greater than 90%. The first two vibration periods of the FEM and the uniform FSM are the same, while the relative errors of the third to fifth vibration periods are 4.93%, 12.18%, and 11.33%, respectively. Considering that the sum of the fourth and fifth modal mass participation coefficients is only 6%, which means corresponding structural response contribution of these two modes is slight, the relative error of the vibration periods is acceptable. Table 2 is the corresponding parameters used in the uniform FSM.

Table 1 – Vibration periods and modal mass participation coefficients of first five modes

Model	T_1(s)	$\gamma_{m,1}$	T_2(s)	$\gamma_{m,2}$	T_3(s)	$\gamma_{m,3}$	T_4(s)	$\gamma_{m,4}$	T_5(s)	$\gamma_{m,5}$
FEM	6.14	0.62	1.61	0.18	0.73	0.07	0.43	0.04	0.26	0.02
Uniform FSM	6.14	0.68	1.61	0.12	0.69	0.06	0.37	0.03	0.23	0.02

Table 2 – Parameters used in the uniform FSM

Total weight ($\times10^6$kN)	H (m)	ρ_0 ($\times10^5$kg/m)	α_0	EI_0 ($\times10^{10}$kN·m^2)	GA_0 ($\times10^7$kN)
2.14	258	8.44	3.59	6.42	1.24

2.3 Sensitivity of parameters in uniform FSM

Since ICT, EFC and outriggers are main structural components of the frame-core tube structures with outriggers, the parameter sensitivity analysis mainly includes the flexural stiffness and shear stiffness of the ICT (EI_{ICT} and GA_{ICT}), the flexural stiffness and axial stiffness of the EFC (EI_{EFC} and EA_{EFC}), and the flexural stiffness and shear stiffness of the outrigger (EI_O and GA_O). The variables in the sensitivity analysis are set as 50%, 75%, 125% and 150% of their original values, respectively. In particular, since the EI_O and GA_O of outriggers are both mainly determined by the axial stiffness of the chord members and the DBs, only the EI_O is considered in the parameter analysis. The stiffness change of the structural component is realized by the "property modification" command in ETABS[7]. All the sensitivity coefficients are calculated as the ratio of the relative change of a concerned parameter in the uniform FSM to the relative change of a variable.

The vibration periods and mode shapes of the uniform FSM are uniquely determined with the specific T_1 and α_0. Fig. 5 shows the results of the sensitivity analysis of T_1. It can be observed that EA_{EFC}、EI_{ICT} and EI_O are the most significant three factors to T_1, while the effect of EI_{EFC} is neglectable. With the existence of the outrigger, the axial force in the EFC are increased, which leads to the fact that the resisting moment caused by the axial force in the EFC is much larger than that related to the local bending of the EFC. Such a phenomenon indicates that compared with EI_{EFC}, EA_{EFC} is more important to the structural lateral stiffness of the FCTS with outriggers. Fig. 6 shows the results of the sensitivity analysis of α_0. EA_{EFC} and EI_{ICT} are the two factors that have the greatest influence on the α_0. Different from the result in Fig. 5, it seems that α_0 is not so sensitive to EI_O. It can be explained by the Eq. (1), in which the increasing EI_O not only increases the axial deformation of the EFC with larger axial forces, but also enhances the shear stiffness of EFCs by harder constraints of rotation. When the increasing degrees of EI_0 and GA_0 are close to each other, the value of α_0 does not vary a lot. The results of the sensitivity analysis above show that increasing EI_{ICT} and decreasing EA_{EFC} are the most effective measures to reduce and increase α_0, respectively.

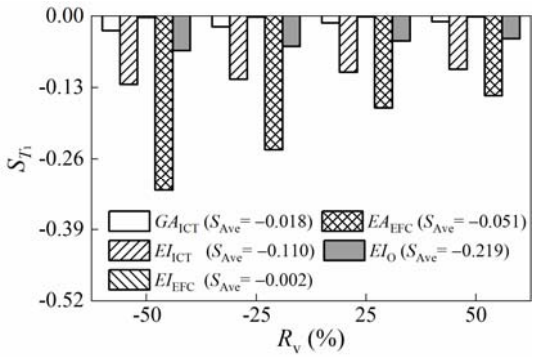

Fig. 5 – Sensitivity of T_1

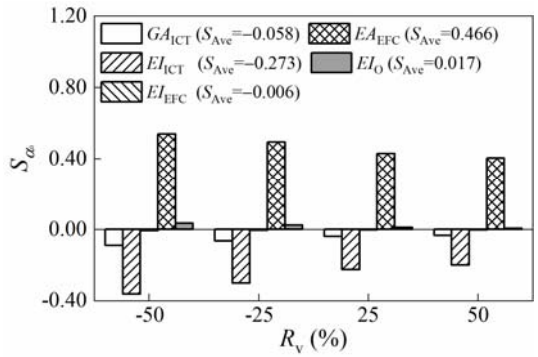

Fig. 6 –Sensitivity of α_0

Specifically, Fig. 7 and Fig. 8 show the sensitivity coefficients of EI_0 and GA_0, respectively. It can be seen that EI_0 is most sensitive to EI_{ICT} with a positive correlation, which indirectly indicates that EI_{ICT} is the primary component of EI_0. The corresponding S_{EI0} of EA_{EFC} is negative, indicating that EI_0 decreases gradually with the increase of EA_{EFC}. It is because the axial deformation of EFC is decreased with higher axial stiffness, making the lateral deformation of the structure gradually deviates from that of a flexural beam. For GA_0, EA_{EFC} is the most important factor. In the analysis of the frame structure, the variation of lateral stiffness caused by the axial deformation of the frame column is often considered in the equivalent shear stiffness of the structure[12], so the exterior frames can be regarded as the main component of GA_0.

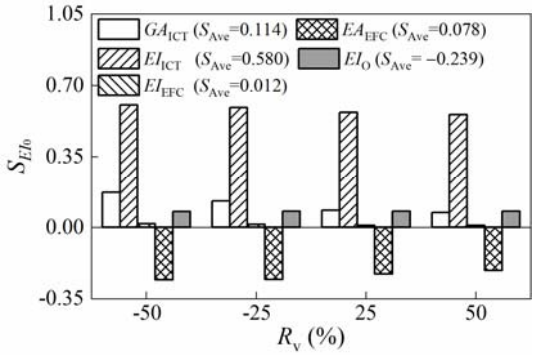

Fig. 7 – Sensitivity of EI_0

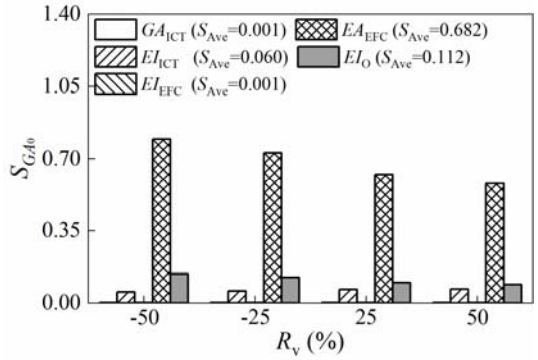

Fig. 8 –Sensitivity of GA_0

2.4 Approximate relations

The vibration periods and the mode shapes of the uniform FSM are uniquely determined with the specific EI_0, ρ_0, H and α_0. Based on previous results of sensitivity analysis of T_1 and α_0, EI_{ICT}, EA_{EFC}, and EI_O are selected as the representative parameters of ICT, EFC, and outriggers. For the constant EI_{ICT}, the following two non-dimensional ratios can be used to determine EA_{EFC} and EI_O:

$$\beta = \frac{2EA_{EFC}L^2}{EI_{ICT}} \tag{5}$$

$$\lambda = \frac{EI_O H}{EI_{ICT} L} \tag{6}$$

Where, L is the maximum horizontal distance from the intersection points of outriggers and EFCs to the centroid axis.

EI_{ICT}, EA_{EFC} and EI_O are estimated as

$$EI_{ICT} \approx E_c \left(\sum_{i=1}^{N_{wx}} \frac{1}{12} A_{w,i} B^2 + \sum_{i=1}^{N_{wy}} \frac{1}{4} A_{w,i} B^2 \right) + E_s \sum_{i=1}^{N_c} 2A_{sc,i} B_{sc,i}^2 \tag{7}$$

$$EA_{EFC} = \sum 2\left[E_s \mu_j + E_c \left(1 - \mu_j\right) \right] A_{c,j} \frac{L_j^2}{L^2} \quad (j = \text{A,B,C,D}) \tag{8}$$

$$EA_{EFC} = \frac{1}{2} \frac{N_s^2}{N_s^2 - 1} EA_b h^2 \tag{9}$$

Where, $A_{w,i}$ is the section area of the i^{th} shear wall parallel or perpendicular to the direction of the earthquake; $A_{sc,i}$ is the section area of the i^{th} steel column; B is the length of shear wall parallel to the direction of the earthquake, i.e. 11.7m; N_{wx} and N_{wy} are the numbers of shear walls parallel and perpendicular to the direction of the earthquake, respectively; N_c is the number of steel columns; $B_{sc,i}$ is the distance from the i^{th} steel column to the centroid axes; $A_{c,j}$, μ_j and L_j are the section area, steel ratio and distance to the centroid axis respectively; EA_b is the axial stiffness of chord beams of outriggers; h is the height of the strengthened story; N_S is the number of spans of outriggers; E_c and E_s are the elastic modulus of concrete and steel, respectively.

In Eq. (9), EA_{EFC} is the sum of the axial stiffness of different EFCs converted based on the principle that the inertia moment to the centroid axes keeps constant. Moreover, EI_{ICT} and EA_{EFC} take the averages calculated by the values at the top and bottom stories. Fig. 9 shows the relation between EI_{ICT}/EI_0 and β with different λ, where λ_0 is the λ value of the original model. With the increase of β, the proportion of the flexural

deformation caused by the axial deformation of EFC in the overall flexural deformation of the structure decreases gradually, thus EI_{ICT}/EI_0 increases gradually. Besides, because outriggers facilitate the cooperative work of ICT and EFC, EI_{ICT}/EI_0 decreases with the increase of λ. Fig. 10 shows the relation between α_0 and β with different λ. It can be seen that compared with λ, α_0 is more sensitive to β.

The following regression formulas can be obtained based on the data in Fig. 9 and Fig. 10:

$$\frac{EI_{ICT}}{EI_0} = a + \frac{1-a}{1+\mathrm{e}^{-b-4\ln\beta}} \tag{10}$$

$$\alpha_0 = c - d\mathrm{e}^{-f\beta} \tag{11}$$

Where, a, b, c, d, and f are regression coefficients, a=0.63/(1-0.2587e$^{-2.469\lambda}$)，b=-3.702λ^2-0.6144λ-6.415，$c = 8.534\left(1-0.4262\mathrm{e}^{-15.53\lambda^{2.1}}\right)$，$d$=11.16$\lambda$+2.836 和 f=0.2057e$^{-2.715\lambda}$.

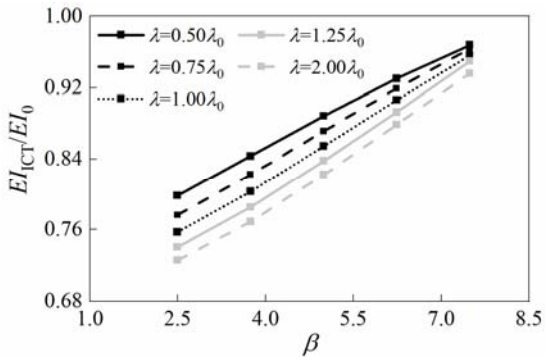

Fig. 9 – EI_{ICT}/EI_0 with different β

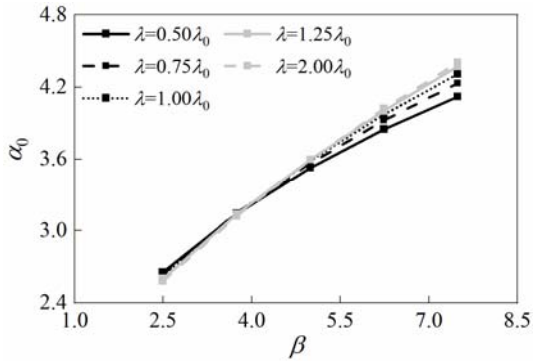

Fig. 10 – α_0 with different β

Eq. (10) and Eq. (11) reflect the following phenomenons: 1) when β approaches zero, the axial deformation of EFC tends to be infinite, and α_0 tends to a fixed value; 2) When β approaches infinity, the axial deformation of EFC can be ignored, while the corresponding overall overturning moment is mainly resisted by the ICT, thus EI_{ICT}/EI_0 approaches 1; 3) When λ approaches zero, the resistance of EFC cannot be ignored because of capacity of the connecting beams between EFC and ICT to transmit internal forces. Corresponding α_0 tends to a fixed value greater than zero; 4) As λ goes to infinity, α_0 also tends to a fixed value greater than zero.

3. Preliminary design strategy based on the target OMRF$_0$ and maximum EIDR

3.1 Statistical relation between vibration periods and structural height

Although structural vibration properties are affected by various factors, there is still a close relation between them and the structural height. Such relation can be more clarified through a regressive analysis based on collected relevant statistical data. It must be acknowledged that the data of higher-order vibration periods are still limited. Thus, only the first two periods are adopted to build such relation. A total of 124 super high-rise frame core-tube buildings with H varying between 100m and 600m are selected from the reference by Xu et al.[13]. As shown in Fig. 11, the fundamental vibration periods of these buildings are distributed within the range of 3s and 9s, exhibiting a large scatter. The regression formula of T_1 is shown as follows:

$$T_1 = 0.1026H^{0.712} \tag{12}$$

As indicated by Fig. 11, the regression is acceptable with an R-squared of R^2=0.7926. As for T_2/T_1, a lower bound and an upper bound can be clearly observed from Fig. 12. They can be approximated desirably by the prediction interval of 95% confidence level (CL), i.e.

$$\left(T_2/T_1\right)_{\mathrm{L}} = 0.123H^{0.120} \tag{13}$$

$$\left(T_2/T_1\right)_{\mathrm{U}} = 0.179H^{0.120} \tag{14}$$

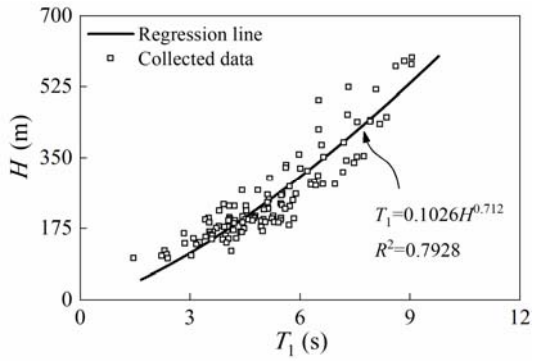

Fig. 11 – Nonlinear curve fitting of relation between T_1 and H

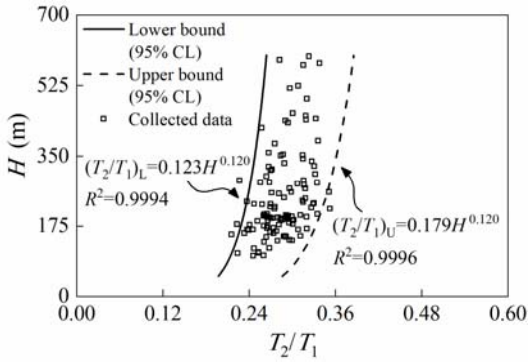

Fig. 12 – Nonlinear curve fitting of relation between T_2/T_1 and H

3.2 Design-spectrum-based elastic inter-story drift ratio estimate

The sesimic EIDR can be estimated by combining the mode decomposition method and the design response spectrum.The EIDR of the n^{th} story corresponding to the i^{th} mode can be estimated by

$$EIDR_i\left(x_n\right) \approx \frac{\Gamma_i T_{i\ i}^2 S_{\mathrm{a},i}}{4\pi^2 H}\phi_i'\left(\frac{x_n + x_{n-1}}{2}\right) \tag{15}$$

Where, $x_{n\text{-}1}$ and x_n are the normalized heights of the $(n\text{-}1)^{\mathrm{th}}$ story and the n^{th} story, respectively; $\phi'_i(x_n/2+x_{n\text{-}1}/2)$ is the derivative of the i^{th} modal shape at the average level of the n^{th} story; $S_{\mathrm{a},i}$ is the spectral acceleration at T_i; Γ_i is the modal participation coefficient of the i^{th} mode.

The derivative of the i^{th} mode shape of the uniform FSM is shown as follows[3]:

$$\phi_i'(x) = \frac{\chi_i\cos\left(\chi_i x\right) - \gamma_i\cosh\left(x\sqrt{\alpha_0^2+\chi_i^2}\right) + \nu_i\left[\sqrt{\alpha_0^2+\chi_i^2}\sinh\left(x\sqrt{\alpha_0^2+\chi_i^2}\right) + \chi_i\sin\left(\chi_i x\right)\right]}{\sin\lambda\left(\chi_i\right) - \gamma_i\left(\alpha_0^2+\chi_i^2\right)^{-1/2}\sinh\left(\sqrt{\alpha_0^2+\chi_i^2}\right) + \nu_i\left[\cosh\left(\sqrt{\alpha_0^2+\chi_i^2}\right) - \cos\left(\chi_i\right)\right]} \tag{16}$$

Where, H is total structural height; x is normalized height with the respect of the base of a structure of concern, x=z/H; ν_i is a non-dimensional parameter

$$\nu_i = \frac{\chi_i^2\sin\left(\chi\right) + \chi_i\sqrt{\alpha_0^2+\chi_i^2}\sinh\left(\sqrt{\alpha_0^2+\chi_i^2}\right)}{\chi_i^2\cos\left(\chi_i\right) + \left(\alpha_0^2+\chi_i^2\right)\cosh\left(\sqrt{\alpha_0^2+\chi_i^2}\right)} \tag{17}$$

The complete quadratic combination (CQC) rule[14] can be applied to provide a estimate on the EIDR considering the influence of multiple modes, i.e.

$$EIDR\left(x_n\right) = \sqrt{\sum_{i=1}^{N_{\mathrm{m}}}\sum_{j=1}^{N_{\mathrm{m}}}\rho_{ij}EIDR_i\left(x_n\right)EIDR_j\left(x_n\right)} \tag{18}$$

Where, N_m is the mode number, whose minimum value should satisfy the requirement that the cumulative modal mass participation coefficient is not less than 90%[8]; ρ_{ij} is the correlation coefficient between the i^{th} and the j^{th} modes, defined by[8]

$$\rho_{ij}=\frac{8\zeta^2\left(1+\kappa_{ij}\right)\kappa_{ij}^{3/2}}{\left(1-\kappa_{ij}^2\right)^2+4\zeta^2\kappa_{ij}\left(1+\kappa_{ij}\right)^2+8\zeta^2\kappa_{ij}^2} \tag{19}$$

Where, κ_{ij} the period ratio of the i^{th} and j^{th} vibration periods, i.e. $\kappa_{ij}=T_i/T_j$; ζ is the damping ratio for all modes.

To the example structure in 2.1, the maximum EIDRs estimated by the FEM and uniform FSM is 0.0034 and 0.0030, respectively. The relative error, i.e. about 10%, may be caused by the assumption of uniform mass and stiffness.

3.3 $OMRF_0$ estimate

The SM, a classical model to estimate structural responses of the FCTS, is adopted here. Since the $OMRF_0$ mains depends on the structural system rather than the load type, the inverted triangle load, a frequently-used pattern of the equivalent seismic force in the preliminary structural design, is used here to provide an analytical solution to the $OMRF_0$. Based on the internal forces under the inverted triangle load provided by Zhou et al.[15] the $OMRF_0$ can be derived as follows:

$$OMRF_0=1-\frac{1}{8\left(1+\frac{1}{\beta}\right)}\{1,1,\cdots,1\}\begin{bmatrix} w+(1-\xi_1) & 1-\xi_2 & \cdots & 1-\xi_n \\ 1-\xi_2 & w+(1-\xi_2) & \cdots & 1-\xi_n \\ \vdots & \vdots & \ddots & \vdots \\ 1-\xi_n & 1-\xi_n & \cdots & w+(1-\xi_n) \end{bmatrix}^{-1}\begin{bmatrix} 3-4\xi_1^3+\xi_1^4 \\ 3-4\xi_2^3+\xi_2^4 \\ \vdots \\ 3-4\xi_n^3+\xi_n^4 \end{bmatrix} \tag{20}$$

Where, ξ_n is the normalized distance from the outrigger to the top of the structure; $w=S_H/S_V$, $S_H=(W/L)^2[W/(24EI_O)+1/(2hGA_O)]$, $S_V=H[1/EI_{ICT}+1/(2EA_{EFC}L^2)]$, W is the maximum horizontal distance from the intersections of outriggers and EFCs to the intersections of outriggers and ICT.

Eq. (7) to Eq. (9) are adopted to estimate $OMRF_0$ in Eq. (20). To the example structure in 2.1, the FEM-based $OMRF_0$s under the inverted triangle load and the spectrum-based seismic force calculated is 59.00% and 58.76%, respectively, which further demonstrates that the $OMRF_0$ is independent of the load pattern. The $OMRF_0$ estimated by Eq. (20) is 48.19%, which is about 83% of the FEM-based $OMRF_0$s, indicating the $OMRF_0$ estimated by Eq. (20) is conservative to the lower limit of $OMRF_0$ required in the seismic code[8]. The $OMRF_0$s estimated by the FEM without the connecting beams under the inverted triangle load is 55.39%, which is only 6.12% relatively smaller than that estimated by the original FEM. Such a result indicates the integrated effect of the connecting beams between the EFC and the ICT is not the main reason for the relative error estimated by the SM.

3.4 Design process

Fig. 13 is the two-stage design process to achieve the target maximum EIDR and $OMRF_0$. Linear density ρ_0 and structural height H are known. In addition to the several parameters of the structural system and the design response spectrum, the input parameters include the lower limit and upper limit of λ, i.e. λ_L and λ_U, the maximum allowable areas of ICT and EFC at the bottom of the structure, i.e. $[A_{ICT,0}]_{max}$ and $[A_{EFC,0}]_{max}$, target maximum EIDR, i.e. $[EIDR]_{target}$, and target $OMRF_0$, i.e. $[OMRF_0]_{target}$. Since the excessive stiffness of the strengthened story may lead to the formation of the weak story, the target $OMRF_0$ is achieved by increasing λ gradually. Taking the structure in 3.1 as an example, several input parameters are shown as follows: $[EIDR]_{target}=0.002$, $[OMRF_0]_{target}=30\%$, $[A_{EFC,0}]_{max}=3.24m^2$, $[A_{ICT,0}]_{max}=180m^2$,$\lambda_L=0.05$, $\lambda_U=0.50$. With the assumption that the lengths, positions, and materials of the shear walls keep constant, it can be seen from Eq. (7) that EI_{ICT} is proportional to the thickness of the shear wall, which means that it is also proportional to A_{ICT}. Therefore, $A_{ICT,0}$ can be obtained by magnifying the value in the example structure according to the ratio of the two EI_{ICT}. Similarly, $A_{EFC,0}$ can be obtained by magnifying the value in the example structure according to the ratio of the two EA_{EFC}. The design results obtained through the

preliminary design process in Fig. 11 are shown in Table 4. It can be seen that the $OMRF_0$ and maximum $EIDR$ of the designed structure is equal to the expected values, which demonstrates the feasibility of the proposed design process.

Table 4 – Parameters of structure designed based on target $OMRF_0$ and maximum EIDR

T_1 (s)	ρ_0 ($\times 10^5$kg/m)	α_0	EI_0 ($\times 10^{11}$kN·m^2)	GA_0 ($\times 10^7$kN)	$[EIDR]_{max}$	EI_O ($\times 10^8$kN·m^2)	EA_{EFC} ($\times 10^8$kN)	EI_{ICT} ($\times 10^{11}$kN·m^2)	$OMRF_0$
4.76	8.44	2.95	1.39	1.82	0.002	5.51	3.90	1.16	0.30

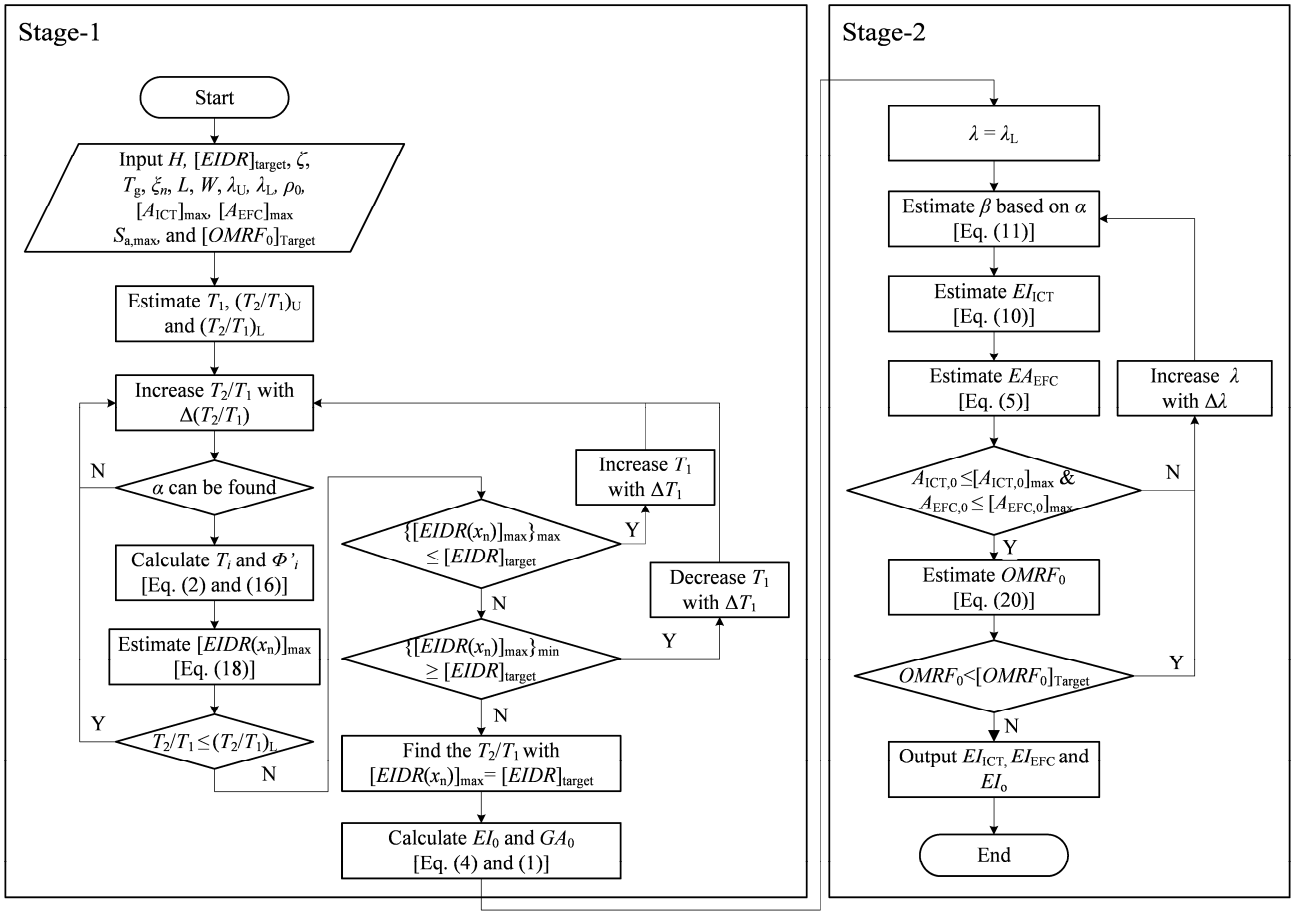

Fig. 13 – Design process based on the targeted $OMRF_0$ and maximum EIDR

4. Conclusion

A two-stage seismic design strategy for the stiffness of the outrigger is proposed to achieve target maximum EIDR and $OMRF_0$. Several conclusion are summarized as follows:

1) The approximate relations between the uniform FSM and the FCTS is proposed. EI_{ICT} is the primary component of the stiffness of flexural beam EI_0. EA_{EFC} and EI_{ICT} are the most important two factors affecting structural overall lateral stiffness and the shape of lateral deformation.

2) A two-stage design process for the stiffness of outriggers is proposed to achieve the target maximum EIDR and $OMRF_0$. Such an efficient process simplifies the design space by reducing the number of constraint functions in each stage, which also makes the stiffness design of the outrigger more reasonable.

3) To realize the design process of this paper, some assumptions are introduced to estimate the maximum EIDR and $OMRF_0$. The non-uniformity of the FSM and the SM should be considered in future research to extend the design process in this paper to super high-rise buildings with structural planes that vary along the height.

Acknowledgements

The authors would like express their gratitude to the financial support from the National Natural Science Foundation of China (Grant No. 51878123), the Fundamental Research Funds for the Central Universities (Grant No. DUT19G208), and the CMEC Special Science and Technology Incubation Project (Grant. No. CMEC-KJFH-2018-01).

References

[1] Wu J R, Li Q S (2003): Structural performance of multi-outrigger-braced tall buildings. The structural design of tall and special buildings, **12** (2), 155-176.

[2] Khan F R, Sbarounis J A (1964): Interaction of shear walls and frames. *Journal of the Structural Division*, **90** (3), 285-335.

[3] Miranda E, Taghavi S (2005): Approximate floor acceleration demands in multistory buildings. I, Formulation. *Journal of Structural Engineering*, **131** (2), 203-211.

[4] Miranda E, Akkar S (2006): Generalized inter-story drift spectrum. *Journal of Structural Engineering*, **132** (6), 840-852.

[5] Alonso-Rodríguez A, Miranda E (2015): Assessment of building behavior under near-fault pulse-like ground motions through simplified models. *Soil Dynamics and Earthquake Engineering*, 79, 47-58.

[6] Alonso-Rodríguez A, Miranda E (2016): Dynamic behavior of buildings with non-uniform stiffness along their height assessed through coupled flexural and shear beams. *Bulletin of Earthquake Engineering*, **14** (12): 3463-3483.

[7] Computers and Structures, Inc (2019): ETABS. https://www.csiamerica.com/categories/etabs.

[8] Ministry of Housing and Urban-Rural Development of the People's Republic of China (2010): *Code for Seismic Design of Buildings (GB50011-2010)*. China Architecture and Building Press, Beijing, China. (in Chinese)

[9] Urban Construction and Traffic Committee of Shanghai (2013): *Code for Seismic Design of Buildings (DGJ08-9-2013)*. Shanghai, China. (in Chinese)

[10] Miranda E (1999): Approximate lateral deformation demands in multistory buildings. *Journal of Structural Engineering*, **125** (4), 417-425.

[11] Xiong C, Lu X, Guan H, Xu Z (2016): A nonlinear computational model for regional seismic simulation of tall buildings. *Bulletin of Earthquake Engineering*, **14** (4), 1047-1069.

[12] Smith B S, Coull A (1991): *Tall Building Structures: Analysis and Design.* John Wiley & Sons, Inc, USA.

[13] Xu P, Xiao C, Li J (2014): Study on relationship between natural vibration periods and heights of structures for high-rise buildings and its reference range. *China Civil Engineering Journal*, **47** (2), 1-11. (in Chinese)

[14] Rosenblueth E and Elorduy J (1969): Responses of linear system to certain transient disturbances. *Proc., the Fourth World Conference on Earthquake Engineering,* Santiago, Chile, **1**, 185-196.

[15] Zhou Y, Zhang C, Lu X (2016): An inter- story drift- based parameter analysis of the optimal location of outriggers in tall buildings. *The Structural Design of Tall and Special Buildings*, **25** (5): 215-231.

